NJC

PAPER

View Article Online
View Journal | View Issue

Cite this: *New J. Chem.*, 2017, **41**, 10132

Vibrational and conformational studies of 1,3-diaminopropane and its N-deuterated and N-ionised derivatives†

Sofia R. O. Mendes,[a] Ana M. Amado,[a] John Tomkinson,[b] M. Paula M. Marques[ac] and Luís A. E. Batista de Carvalho*[a]

Received 11th March 2017,
Accepted 31st July 2017

DOI: 10.1039/c7nj00810d

rsc.li/njc

A vibrational and conformational analysis of the linear alkylpolyamine 1,3-diaminopropane (1,3-dap) is reported, using vibrational spectroscopy (Raman, Fourier Transform Infrared (FTIR) and inelastic neutron scattering (INS)) coupled to theoretical approaches at the Density Functional Theory (DFT) level. The quantum mechanical calculations were carried out using the mPW1PW functional and the 6-31G* basis set, for the isolated molecule, the condensed phase, and solutions in both water and carbon tetrachloride. The most stable geometries were calculated to be GGG′G and TG′GG′ for the gaseous phase and the CCl_4 solution, and TTTT, TGTT and TTTG for the condensed phase and the aqueous solution. Since the relative populations obtained for the different 1,3-dap conformers were very similar, the corresponding experimental spectra reflect the presence of a mixture of species. The vibrational data obtained for 1,3-dap in its pure form – unprotonated, totally protonated (N-ionised) and N-deuterated – as well as for its aqueous and CCl_4 solutions, were assigned in the light of the theoretical results presently obtained and experimental data previously gathered for similar compounds.

Introduction

Rotational isomerism in linear alkylamines that has been the subject of various studies[1–17] is influenced by different factors, from steric and dipolar effects to hyperconjugative and hydrogen bonding interactions.[5,9,11,14] Moreover, the stability of this kind of system is strongly dependent on the balance between intra and intermolecular interactions.[8–10,16–18]

Although polyamine crystals were found in human seminal liquid by Leeuwenhoek about three hundred years ago, only very recently has the biological importance of these compounds been acknowledged. In fact, both 1,3-diaminopropane ($H_2N(CH_2)_3NH_2$, 1,3-dap) and 1,4-diaminobutane ($H_2N(CH_2)_4NH_2$, 1,4-dab, putrescine) are precursors of the biogenic tri- and tetramines spermidine ($H_2N(CH_2)_3NH(CH_2)_4NH_2$, spd) and spermine ($H_2N(CH_2)_3NH(CH_2)_4NH(CH_2)_3NH_2$, spm), which play key physiological functions, namely in eukaryotic cell proliferation and differentiation. Since changes in their biological levels are known to be responsible for a significant effect on cellular proliferation and DNA replication, intracellular polyamine levels are related to carcinogenesis and neoplastic growth.[19] To date, several studies have reported different biological functions for 1,3-dap, namely, a regulator of ornithine decarboxylase (ODC, one of the main enzymes involved in the polyamine biosynthetic pathway)[20,21] and a carcinogen biomarker.[22,23] However, the exact nature of the mechanisms involved, at a molecular level, is still unknown, which highlights the relevance of gathering detailed structural and conformational information on this compound, in order to understand its main biochemical role. Actually, few structural and spectroscopic studies have been performed for this system and even these are limited to narrow regions of the vibrational spectra.[18,24,25] 1,3-dap is also quite relevant at an industrial level, namely in food and pharmaceutic industries. Regarding the latter, it may be used for the design of new diuretic[26] and anticancer[27–30] drugs.

Cancer is one of the pathologies with the greatest impact on society, responsible for a high annual mortality rate.[31] Currently, cisplatin (*cis*-diamminedichloroplatinum(II)) is one of the most widely used and effective chemotherapeutic agents.[32,33] However, it acts in a narrow range of tumours and is associated with severe side effects such as neurotoxicity,[34] ototoxicity[35] and nephrotoxicity,[36] as well as with acquired resistance that limits its prolonged clinical administration. To overcome these limitations and mitigate the deleterious side effects of chemotherapy is a challenging goal that may be

[a] *Unidade de I&D "Química-Física Molecular", Department of Chemistry, University of Coimbra, 3004-535 Coimbra, Portugal. E-mail: labc@ci.uc.pt; Fax: +351-239-826541; Tel: +351-239-854462*

[b] *ISIS Facility, STFC Rutherford Appleton Laboratory, Chilton, Didcot, OX 11 0QX, UK*

[c] *Department of Life Sciences, University of Coimbra, Portugal*

† Electronic supplementary information (ESI) available. See DOI: 10.1039/c7nj00810d

achieved through the rational design of new anticancer agents, namely polynuclear platinum and palladium complexes with linear polyamines (biogenic polyamines and their analogues). In fact, these types of Pt(II) and Pd(II)-polyamine chelates were shown to display promising cytotoxic properties *via* an unconventional interaction with DNA.[27–30,33,37–44]

With a view to understand both the antitumor activity of these compounds and the structural dependence of such activity, it is crucial to have deep knowledge of their aliphatic ligands. Hence, the present work aimed at a conformational study of 1,3-dap, one of the smallest diamines, as well as its N-ionised derivative, using DFT methods and vibrational spectroscopy (both optical – Raman and FTIR – and neutron scattering techniques). The changes in the corresponding conformational equilibria induced by different media polarities were evaluated. In order to assist the assignment of the vibrational spectra, the N-deuterated species $[ND_2(CH_2)_3ND_2]$ were prepared and analysed.

Experimental

Chemicals

1,3-Diaminopropane (>99%), 1,3-diaminopropane dihydrochloride (>98%), carbon tetrachloride (99.9%) and deuterium oxide (99.9 atom% D) were obtained from Sigma-Aldrich (Sintra, Portugal).

1,3-Dap-N-d_4 and $[1,3\text{-dap-N-}d_6]^{2+}\cdot 2Cl^-$ were prepared by repeatedly stirring (three times for *ca.* 1 h at room temperature) a mixture of either 1,3-dap-N-h_4 or $[1,3\text{-dap-N-}h_6]^{2+}\cdot 2Cl^-$ and D_2O (*ca.* 10% excess), followed by distillation using a V-800 Büchi Vacuum Controller (50 mbar; 323 K). Purification of the samples was carried out shortly before running the spectra: the liquids were distilled under vacuum while the salts were recrystallized (sometimes repeatedly) from ethanol : water (1 : 1) (being obtained as white needles). Air or moisture sensitive samples (both the uncharged and the deuterated amines) were always kept on molecular sieves and handled in a glovebox, under a nitrogen or argon atmosphere.

Vibrational spectra

Raman spectroscopy. Raman spectra were obtained on a triple monochromator Jobin-Yvon T64000 Raman system (focal distance 0.640 m, aperture *f*/7.5) equipped with holographic gratings of 1800 grooves mm^{-1}. The premonochromator stage was used in the subtractive mode. The detection system was a liquid nitrogen cooled non-intensified 1024 × 256 pixel (1″) Charge Coupled Device (CCD) chip. A Coherent (model Innova 300-05) Ar^+ laser was used as the light source, the output of which at 514.5 nm was adjusted to provide *ca.* 80 mW at the sample position. A 90° geometry, between the incident radiation and the collecting system, was employed. The entrance slit was set to 200 μm. An integration time of 3 s and 10–15 scans were used in all experiments.

In order to record the low-temperature Raman spectra of 1,3-dap and 1,3-dap-N-d_4 (240 K, solid phase) a home-made Harney-Miller type assembly was used, and the temperature was monitored by the resistivity of a calibrated thermocouple.

Samples were sealed in Kimax glass capillary tubes of 0.8 mm inner diameter. Under the above-mentioned conditions, the error in wavenumbers was estimated to be within 1 cm^{-1}.

FTIR spectroscopy. The Fourier transform infrared (FTIR) spectra were recorded in a Bruker Optics Vertex 70 FTIR spectrometer purged by CO_2-free dry air, in the 400–4000 cm^{-1} range, using KBr disks (*ca.* 0.5% (w/w)). A Ge on KBr substrate beamsplitter and a liquid nitrogen cooled Mercury Cadmium Telluride (MCT) detector were used. The spectra were collected for 2 minutes (*ca.* 140 scans), at a 2 cm^{-1} resolution, and the 3-term Blackman–Harris apodization function was applied. Under these conditions, the accuracy in wavenumbers was well below 1 cm^{-1}.

INS spectroscopy. Inelastic neutron scattering is particularly useful for the study of this kind of hydrogenated compound, yielding complementary information to that obtained from Raman and FTIR since it allows the observation of some low frequency modes unavailable to the optical techniques. The neutron scattering cross-section of an atom (σ) is characteristic of that atom and independent of its chemical environment, with the value for hydrogen (80 barns) far exceeding that of all other elements (*ca.* 5 barns). Hence, the INS spectra are dominated by the vibrational modes involving a significant hydrogen displacement (u_i), and the intensity from a powdered sample at energy ν_i is represented by

$$S_i^*(Q,\nu_k) = \frac{(Q^2u_i^2)\sigma}{3}\exp\left(-\frac{Q^2\alpha_i^2}{3}\right) \quad (1)$$

where Q ($Å^{-1}$) is the momentum transferred from the neutron to the sample and α_i (Å) is associated with a weighted sum of all the displacements of the atom. Therefore, experimental data provide the energies of the vibrational transitions (the eigenvalues, ν_i) as well as the atomic displacements (the eigenvectors, u_i). Additionally, the spectral intensities can be quantitatively compared with DFT-calculated values, allowing us to relate molecular geometry (calculated results) with the experimental spectroscopic features, thus providing a reliable conformational insight of the system under study.

The INS spectra were obtained in the TOSCA spectrometer[45,46] at the ISIS Pulsed Neutron Source of the STFC Rutherford Appleton Laboratory (United Kingdom). This is an indirect geometry time-of-flight, high resolution ($(\Delta E/E)$ *ca.* 1.25%), broad range spectrometer. The compounds (2 to 3 g for the solids and *ca.* 5 mL for the liquids) were placed in thin walled aluminium cans, which filled the beam (4 × 4 cm). To reduce the impact of the Debye–Waller factor (the exponential term in eqn (1)) on the observed spectral intensity, the samples were cooled to cryogenic temperatures (*ca.* 10 K).

Quantum mechanical calculations

The quantum mechanical calculations were carried out using the GAUSSIAN program package[47] within the Density Functional Theory (DFT) approach. The mPW1PW method, which comprises a modified version of the exchange term of Perdew–Wang and the Perdew–Wang 91 correlation functional[48,49] was used, along

with the all-electron double-zeta split valence basis set 6-31G(d).[50]

All different permutations of skeletal dihedral angles – 60° (*gauche*, G), 180° (*trans*, T) or −60° (*gauche*′, G′) – were considered in the definition of the starting geometries for optimization, which was performed without any symmetry constraints, with the following convergence criteria for the cutoffs of forces and step sizes: 0.000015 Hartree $Bohr^{-1}$ for maximum force, 0.000010 Hartree $Bohr^{-1}$ for root-mean-square force, 0.000060 Bohr for maximum displacement and 0.000040 Bohr for root-mean-square displacement.

The harmonic vibrational wavenumbers, as well as the Raman activities and infrared intensities, were obtained at the same level of theory as the geometry optimization, in order to confirm that the geometries correspond to a real minimum in the potential energy surface (no negative eigenvalues) as well as to estimate the zero-point vibrational energy (ZPVE) and the thermal corrections. The obtained wavenumber values were scaled according to Merrick *et al.*:[51] 0.9499 and 0.9828, respectively, above and below 500 cm^{-1}.

In order to simulate the pure liquid phase, and the aqueous and carbon tetrachloride solutions, self-consistent reaction field (SCRF) calculations were performed considering the tabulated dielectric constants at 25 °C (ε = 10.9, 78.39 and 2.228 for 1,3-DAP, H_2O and CCl_4, respectively). The polarisable continuum model (PCM) approach was used with the simple united atom topological model option (UA0) to set the atomic radii, as implemented in GAUSSIAN.[47]

Moreover, aiming at verifying the reliability of the conformational energy differences obtained using the mPW1PW/6-31G(d) method, both wB97XD[52] long-range-corrected and M06-2X[53] meta-hybrid functionals, in conjunction with the all-electron triple-zeta split valence (TZVP) basis set, were used. Additionally, energy single point calculations on the DFT optimised geometries using coupled cluster singles and doubles (triple) [CCSD(T)][54] (often considered as the computational chemistry "gold standard"), along with 6-311++G(2d,p), were performed.

Results and discussion

DFT conformational analysis

H_2N-CH_2-CH_2-CH_2-NH_2. 1,3-dap can adopt different conformations, mainly by varying the dihedral angles around the N^1–C^4, C^4–C^7, C^7–C^{10} and C^{10}–N^{13} bonds (Fig. 1).

Table 1 comprises the conformational energy differences, populations, thermochemical data and dipole moments obtained using DFT calculations, for twenty three conformations of this compound. The estimation of the ΔE-based populations, assuming similar entropy contributions to the free energy of the distinct conformers, is not strictly correct since differences of up to 3.40 kJ mol^{-1} were found for the entropy term ($T\Delta S$). Thus, ΔG-based populations at 298.15 K, calculated according to the Boltzmann law, are also presented in Table 1.

Conformations TGG′T and GGG′G′ were not found to be potential energy surface minima, since some of their calculated vibrational frequencies were imaginary (negative). Singularly, this result was only obtained for the isolated molecule, *i.e.*, when solvent effects were considered, using the SCRF-PCM approach, these geometries were shown to be true energy minima (see below).

The most populated geometries were GGG′G (28%) and TG′GG′ (20%), for which intramolecular (N)H···N hydrogen bonds can be established (Fig. 1). The remaining conformers have calculated populations of less than 7%. Thus, it is possible to predict that the 1,3-dap gas phase system should contain different conformers in simultaneous equilibria with a predominance of the GGG′G and TG′GG′ geometries.

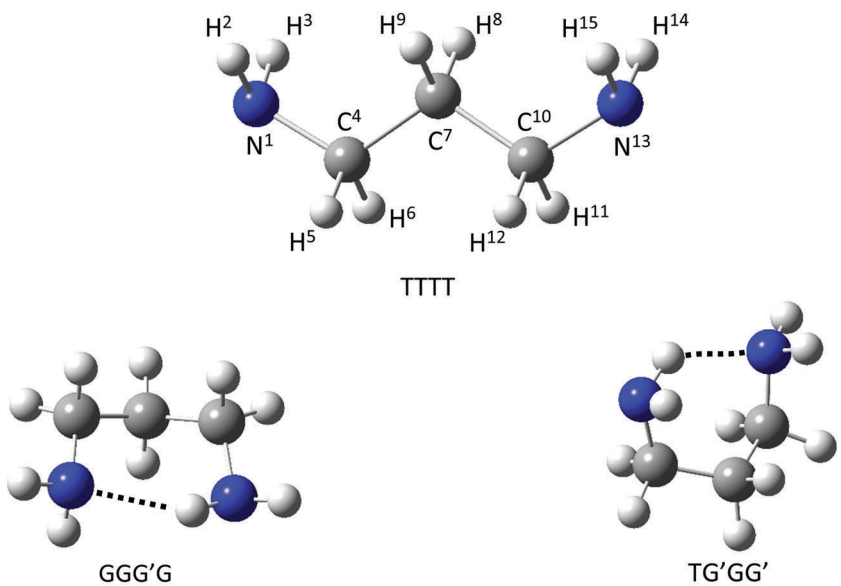

Fig. 1 Schematic representation of some conformers of 1,3-diaminopropane.

Table 1 Calculated (mPW1PW/6-31G*) conformational energies, populations (P_i), thermochemical data (at 298.15 K and 1 atm) and dipole moments (μ) of 1,3-dap conformers

Conformer[a]	S_i	ΔE (kJ mol^{-1})	ΔE_{zpve}[b] (kJ mol^{-1})	$P_i(\Delta E_{zpve})$[c] (%)	ΔH (kJ mol^{-1})	$T\Delta S$ (kJ mol^{-1})	ΔG (kJ mol^{-1})	$P_i(\Delta G)$[d] (%)	μ[e] (D)
GGG′G	2	0.00	0.00	28.0	0.00	0.00	0.00	19.8	1.80
TG′GG′	2	1.03	0.84	19.8	0.96	0.32	0.64	15.2	3.21
TGGG′	2	4.04	3.47	6.7	3.90	1.61	2.30	7.7	2.90
TTTT	1	5.39	3.57	3.2	4.74	1.22	3.52	2.3	2.04
GGGG′	2	4.28	4.32	4.7	4.63	0.96	3.67	4.4	1.76
GG′G′G	2	5.94	4.37	4.6	5.17	2.06	3.11	5.5	0.86
TTGG′	2	6.44	4.45	4.5	5.50	2.94	2.56	6.9	2.89
TTTG	2	6.65	4.67	4.1	5.91	3.17	2.74	6.4	1.77
TGTT	2	6.41	4.69	4.0	5.65	2.61	3.04	5.6	1.64
GTGG′	2	6.92	5.18	3.3	6.13	2.57	3.57	4.5	1.41
TGTG	2	7.25	5.54	2.8	6.50	2.66	3.84	4.1	1.80
TGGT	2	6.54	5.62	2.7	6.20	0.12	6.09	1.6	1.27
GTTG	2	8.20	6.25	2.1	7.50	1.46	6.04	1.6	1.46
GTG′G	2	8.28	6.39	2.0	7.51	3.23	4.28	3.4	1.63
TTGG	2	7.87	6.43	2.0	7.40	2.60	4.80	2.7	1.69
TGTG′	2	8.47	6.61	1.8	7.63	2.88	4.75	2.8	2.05
GTTG′	1	9.65	7.47	0.6	8.79	3.40	5.39	1.1	2.73
TGGG	2	9.52	7.57	1.2	8.52	2.83	5.69	1.9	1.90
GTG′G′	2	10.05	8.40	0.9	9.49	2.96	6.53	1.3	1.65
GGTG	2	10.92	9.04	0.7	10.15	3.05	7.10	1.1	2.68
GGGG	2	12.29	11.03	0.3	11.92	1.15	10.77	0.2	1.83
TGG′T		15.89	13.38		12.41	−1.79	14.19		1.17
GGG′G′		23.75	20.68		20.02	−0.81	20.84		2.67

[a] See Fig. 1. [b] ΔE_{ZPVE}, zero-point vibrational energy corrected relative energies. [c] Population according to ΔE_{ZPVE} values. [d] Population according to ΔG values. [e] 1 D = $1/3 \times 10^{-29}$ C m.

The conformational stability of a molecule is influenced by various intramolecular effects, including steric, inductive, mesomeric, hyperconjugative, H-bonding and entropic interactions. For 1,3-dap it was found that the latter are particularly important (Table 1). Actually, the relative conformer populations taking into account the Gibbs energy lead to a slight population change: GGG′G (19.8%) and TG′GG′ (15.2%), the remaining conformers accounting for 65% of the total population.

The decrease of the relative GGG′G and TG′GG′ populations, when considering the Gibbs energy, is mainly due to the fact that the entropic component of these two conformations is much smaller than that calculated for all others, for which there is an additional stabilization resulting in positive $T\Delta S$ values, above 1 kJ mol^{-1} (Table 1).

The reliability of these predictions was checked against the CCSD(T) gold standard approach, for the twelve most stable conformers (Table S1, ESI†). It should be stressed that all the methodologies confirm GGG′G as the lowest energy conformation. Despite this, there is no agreement in the ordering of conformational energy differences using different functionals. Furthermore, the root-mean-square deviations (RMSDs) of ΔE present lower values when wB97XD and M06-2X functionals with triple-zeta quality basis sets were used, but the RMSD of ΔG obtained using the mPW1PW/6-31G(d) method displays the lowest value (Table S1, ESI†). These findings support the claim of Padrão *et al.*[14] that mPW1PW/6-31G(d) is a suitable tool to study these kinds of systems.

Table 2 presents the conformational energy differences, populations, thermochemical data and dipole moments for pure (liquid) 1,3-dap, obtained using SCRF-PCM calculations considering 298.15 K and the dielectric constant of the corresponding medium (in this case 1,3-dap itself).

Considering the energy values corrected for the zero-point vibrational energy (ZPVE), the most stable conformation in the condensed phase was found to be TTTT (Fig. 1), with a predicted population of *ca.* 13% at 298 K. In fact, due to the small energy differences between conformers, the system under study should consist of a diversified mix at room temperature. Thus, the presence of the TTTG and TGTT conformers, which have the same energy, is also expected, with approximate populations of 11.5%. All other conformers have populations lower than 7.5% but, as they are in larger number, they are responsible for *ca.* 65% of the total population in the pure liquid phase (Table 2).

When considering the population distribution based on Gibbs energies, this conformer mixture undergoes profound changes, being mostly comprised of TTTG (13.9%) and TGTT (13.1%) species, while the all-*trans* conformation (TTTT) becomes the fifth most populated one (7.5%, Table 2). In fact, this conformer does not display the additional entropic stabilization that occurs in most other conformations which have a positive $T\Delta S$ value (Table 2).

It should, however, be noted that the currently performed calculations only consider intermolecular interactions in the condensed phase in a global manner, through the dielectric constant of the medium, and do not take into account the specific nature of interactions such as intermolecular hydrogen bonds. In this perspective, the three-dimensional structure of the TTTT conformer will enable an interplay between the NH_2 groups of the 1,3-dap molecules, *i.e.* the intermolecular connection between two adjacent molecules, much more easily than, for

Table 2 Calculated (mPW1PW/6-31G*) conformational energies, populations (P_i), thermochemical data (at 298.15 K and 1 atm) and dipole moments (μ) of 1,3-dap conformers in the pure liquid phase simulation (SCRF-PCM)

Conformer[a]	S_i	ΔE (kJ mol^{-1})	ΔE_{zpve}[b] (kJ mol^{-1})	$P_i(\Delta E_{zpve})$[c] (%)	ΔH (kJ mol^{-1})	$T\Delta S$ (kJ mol^{-1})	ΔG (kJ mol^{-1})	$P_i(\Delta G)$[d] (%)	μ[e] (D)
GGG′G	2	3.12	4.59	4.0	3.58	−0.85	4.43	2.4	2.42
TG′G′G′	2	1.51	3.34	6.7	2.28	−0.95	3.23	3.9	3.92
TGGG′	2	3.35	3.78	5.5	3.46	2.25	1.22	9.0	3.48
TTTT	1	0.00	0.00	13.2	0.00	0.00	0.00	7.5	2.55
GGGG′	2	5.82	6.77	1.6	6.28	1.16	5.12	1.8	2.08
GG′G′G	2	6.14	6.02	2.2	5.75	1.18	4.57	2.3	1.45
TTGG′	2	3.36	3.06	7.5	2.99	1.91	1.08	9.5	3.54
TTTG	2	2.27	2.02	11.4	2.07	1.90	0.17	13.9	2.13
TGTT	2	1.83	2.02	11.4	1.83	1.51	0.32	13.1	1.97
GTGG′	2	5.23	4.97	3.4	4.86	1.65	3.21	4.0	1.80
TGTG	2	3.61	3.71	5.7	3.52	1.48	2.04	6.4	2.17
TGGT	2	2.37	3.90	5.3	3.15	−1.42	4.57	2.3	1.33
GTTG	2	4.55	4.19	4.7	4.31	0.32	3.99	2.9	1.83
GTG′G	2	6.30	5.93	2.3	5.93	2.13	3.81	3.1	1.98
TTGG	2	4.38	4.73	3.7	4.51	1.30	3.21	4.0	2.00
TGTG′	2	4.55	4.50	4.1	4.39	1.76	2.63	5.0	2.55
GTTG′	1	5.23	4.75	1.9	4.92	2.20	2.72	2.4	3.41
TGG′G	2	6.08	6.10	2.1	5.88	1.68	4.20	2.6	2.44
GTG′G′	2	7.10	7.13	1.4	7.04	1.69	5.36	1.6	2.10
GGTG	2	6.92	6.93	1.5	6.81	1.58	5.23	1.7	3.36
GGGG	2	9.00	9.80	0.5	9.43	−0.40	9.82	0.3	2.32
TGG′T	1	11.28	11.39	0.1	11.30	2.48	8.82	0.2	1.44
GGG′G′	1	12.58	13.75	0.0	13.12	0.01	13.11	0.0	3.50

[a] See Fig. 1. [b] ΔE_{ZPVE}, zero-point vibrational energy corrected relative energies. [c] Population according to ΔE_{ZPVE} values. [d] Population according to ΔG values. [e] 1 D = $1/3 \times 10^{-29}$ C m.

example, the GGG′G conformer (Fig. 1; more stable in the gas phase) that has a non-linear geometry. In fact, the formation of this type of intermolecular bond is rendered much more difficult for the latter due to steric hindrance factors. The occurrence of intramolecular H-bonds, in turn, is not possible in the TTTT, TTTG and TGTT conformers, thus favouring the intermolecular ones. The additional stabilization of the system caused by these close contacts can have profound implications in the corresponding conformational equilibria.

It should also be mentioned that despite the pronounced changes in the conformational equilibrium due to the effect of the environment – gaseous *vs.* pure liquid – one cannot establish any correlation, either positive or negative, between the energy and dipole moment values for the distinct conformers.

For the simulation of the aqueous solution of 1,3-dap, when considering the population based on the electronic energy (ZPVE corrected), the conformational mixture is composed mainly of the TTTT (15.0%), TGTT (12.2%) and TTTG (12.0%) species. The remaining conformers, with populations below 8%, contribute *ca.* 60% (Table S2, ESI†) to the whole population. When the Gibbs energy is considered some differences are observed, the most prominent one being the decrease of the all-*trans* population, from 15.0% to 8.3% and the increase of conformers TTGG′, from 7.6% to 9.6%, and TGGG′, from 5.3% to 9.4%. The stabilization of the latter is due to a very high value of entropy ($T\Delta S$ = 2.62 kJ mol^{-1}) when compared with the other conformers, in particular the TTTT conformer (Table S2, ESI†).

The water being a polar solvent, its polarity is prone to affect 1,3-dap's conformational stability. It would be expected that the conformations with a higher dipole moment would be favoured in aqueous solution. However this is not the case, with the presence of conformations with an intermediate dipole moment ($\approx$2.2 Debye) being preferred. As mentioned earlier, effects other than the dipole moment appear to be more relevant for determining the conformational stability of this system. Actually, once more no correlation is found between the conformer energies and their calculated dipole moments (Table S2, ESI†).

In turn, for the 1,3-dap/CCl_4 solution it is possible to forecast the existence of two conformations with higher stability, TG′GG′ (14.6%) and GGG′G (13.8%) (Table S3, ESI†; Fig. 1). Nevertheless, there are drastic differences in this conformational equilibrium when the populations are determined considering the Gibbs energy values: six conformers with populations between 8.7 and 10.5% (TTTG, TG′GG′, TGTT, TGGG′, GGG′G and TTGG′; Table S3, ESI†). Note that the most populated conformations considering ΔE_{ZPVE} (TG′GG′ and GGG′G) show negative entropy values (ΔS), *i.e.* in these two conformers the entropic factor plays a destabilising role. Conversely, for conformers TTTG, TGTT, TGGG′ and TTGG′ the $T\Delta S$ value is higher than 2.0 kJ mol^{-1}, which results in an additional stability and very low ΔG values. Since carbon tetrachloride is non-polar, it would be expected that the most stable conformations adopted by 1,3-dap in CCl_4 solution were the less polar ones. Instead, the opposite was observed: three of the most stable conformations display the largest dipole moment values (>3.1 Debye). This evidences that, once again, the dipole moment is not a decisive parameter in the conformational equilibrium of this system.

Table S4 (ESI†) contains the structural parameters for the most stable conformations in each medium considered in the present work. It is possible to conclude that for the same

conformation but different chemical environments, the differences between bond lengths, angles and dihedral angles are negligible. There are no experimental values reported in the literature (X-ray diffraction, neutron diffraction, *etc.*) for a comparison with the values presently obtained. It is believed, however, that there are good estimates for real systems insofar as the methodology has proven very effective in other systems.[14,43]

$[H_3N\text{-}CH_2\text{-}CH_2\text{-}CH_2\text{-}NH_3]^{2+}$. Table 3 presents the conformational energy differences, populations, thermochemical data and dipole moments obtained for different conformations of the 1,3-dap N-ionised derivative ($[1,3\text{-dap-N-h}_6]^{2+}$). Since both amine groups are protonated (NH_3^+), the hydrogen atoms bound to nitrogen are rendered equivalent. Therefore, the conformational analysis becomes much simpler, with the number of possible conformations with minimal energy being drastically decreased. In fact, only three conformers were found, one being much more stable than the others: the all-*trans* conformer (TT) with a population predicted to be *ca.* 99%.

Vibrational analysis

$H_2N\text{-}CH_2\text{-}CH_2\text{-}CH_2\text{-}NH_2$. Fig. 2 comprises the Raman and FTIR spectra of liquid (pure) 1,3-dap, whereas Fig. 3 presents the Raman and INS spectra in its solid phase.

The experimental wavenumbers are presented in Table 4, along with the DFT calculated values for the TTTT conformer (C_{2v} symmetry). In this conformation the molecule displays 39 normal vibrational modes distributed by four symmetry species, as follows: $12A_1 + 8A_2 + 9B_1 + 10B_2$. All these vibrations are Raman- and INS-active, whereas only 31 fundamental modes are expected on the infrared spectra as the eight A_2 vibrations are IR-inactive. Actually, INS being a non-optical vibrational technique it is not subject to the optical selection rules.

The agreement between the experimental and calculated wavenumbers, after scaling according to Merrick *et al.*[51] in order to correct for the anharmonicity of the normal modes of vibration, was found to be rather good (Fig. S1, ESI†). In fact, since the calculated energy differences between the five most

Table 3 Calculated (mPW1PW/6-31G*) conformational energies, populations (P_i), thermochemical data (at 298.15 K and 1 atm) and dipole moments (μ) of $[H_3N\text{-}CH_2\text{-}CH_2\text{-}CH_2\text{-}NH_3]^{2+}$ conformers

Conformer	S_i	ΔE_{zpve}[a] (kJ mol^{-1})	$P_i(\Delta E_{zpve})$[b] (%)	ΔH (kJ mol^{-1})	$T\Delta S$ (kJ mol^{-1})	ΔG (kJ mol^{-1})	$P_i(\Delta G)$[c] (%)	μ[d] (D)
TT	1	0.00	99.6	0.00	0.00	0.00	98.9	1.36
TG	2	14.83	0.4	14.87	2.24	12.63	1.1	2.18
GG	2	27.09	0.0	27.48	3.37	24.10	0.0	1.64

[a] ΔE_{ZPVE}, zero-point vibrational energy corrected relative energies. [b] Population according to ΔE_{ZPVE} values. [c] Population according to ΔG values. [d] 1 D = 1/3 × 10^{-29} C m.

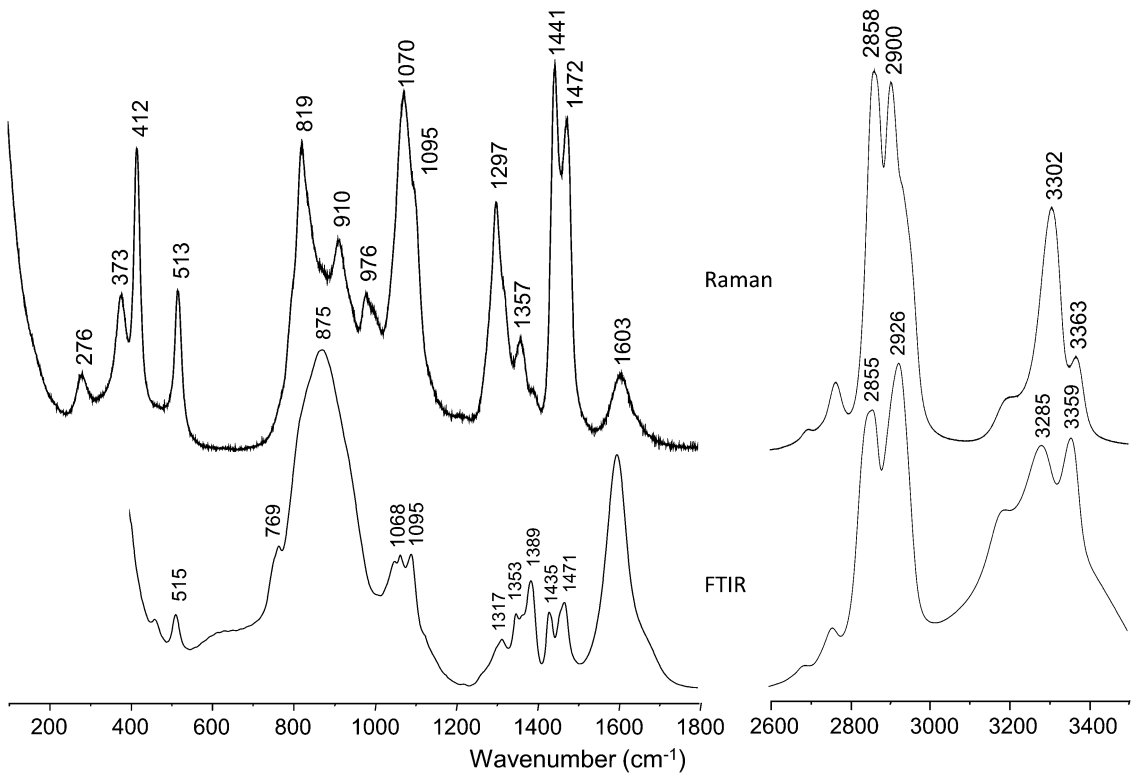

Fig. 2 Raman (100–1800 and 2600–3500 cm^{-1}) and FTIR (400–1800 and 2600–3500 cm^{-1}) spectra of 1,3-diaminopropane in the liquid phase.

stable conformers does not exceed *ca.* 1 kJ mol^{-1}, all of these conformers are significantly populated at room temperature (Table 2). However, the calculated values for the low frequency region (below 600 cm^{-1}), which is the most conformationally sensitive one, are remarkably consistent with the sole presence of conformer TTTT for solid 1,3-dap. Table 4 also contains the complete assignment of 1,3-dap experimental bands to the normal modes of vibration. It is worth mentioning that most of the observed frequencies can be considered as group frequencies, *i.e.* highly localized on a particular group within the molecule.

A full assignment of the vibrational spectra was carried out considering both nondeuterated and N-deuterated samples, as the deuteration clearly evidences which bands correspond to vibrations of the NH_2 groups: (i) in the 3150–3400 cm^{-1} region, the NH_2 symmetric (ν_s) and antisymmetric (ν_{as}) stretching vibrations (Fig. 2 and 3), that are detected at 2350–2550 cm^{-1} for 1,3-dap-N-d_4 (Fig. 4), displaying the expected wavenumber red shift of *ca.* 1.37×; (ii) the scissoring modes of the amine groups (αNH_2) at *ca.* 1600 cm^{-1} (Fig. 2), that deviate to *ca.* 1197 cm^{-1} upon deuteration (Fig. 4); (iii) the NH_2 twisting at 1353 cm^{-1} (Fig. 2), which are observed at 1153 cm^{-1} for the deuterated compound (Fig. 4); (iv) the FTIR broad and intense NH_2 wagging at 875 cm^{-1} (Fig. 2), that is downward shifted (by *ca.* 100 cm^{-1}) in the ND_2 counterpart (Fig. 4); and (v) the amine torsion at 431 cm^{-1}, detected as a shoulder of the longitudinal acoustic mode 1 (LAM1) in the Raman spectrum of solid 1,3-dap (Fig. 3), that emerges as a weak but well defined Raman band at 324 cm^{-1} in solid 1,3-dap-N-d_4 (Fig. 4).

As expected, vibrational modes not directly related to the amine groups do not show comparable wavenumber shifts upon deuteration. However, there are some interesting deviations in the low wavenumber region that should be mentioned. In particular, the bands at 513, 412 and 373 cm^{-1} in the Raman spectrum of liquid 1,3-dap (Fig. 2), assigned to the NCC skeletal deformations, display small displacements to lower wavenumbers in the 1,3-dap-N-d_4 spectrum (23, 14 and 14 cm^{-1}, respectively). Actually, the nitrogen atoms involved in the δNCC modes are linked to deuterium atoms, so that the amine group, considered as a whole, has a greater mass (18 instead of 16 u). Thus, while the force constant remains equal, since it is the same vibrational mode, there is a displacement of the bands due to a mass effect.

The amine wagging vibrations, in turn, are particularly interesting, as they are highly sensitive to the increase of hydrogen bond type interactions in the solid phase:[3] an upward shift of *ca.* 30 cm^{-1} is observed when going from the liquid to the solid, from *ca.* 875 to *ca.* 905 cm^{-1} (Fig. 2 and 3). This vibrational mode, extremely weak in the Raman spectrum, is clearly observed by INS at 908 cm^{-1} (Fig. 3). A similar shift is observed by Raman for the ND_2 wagging mode with A_1 symmetry, at 803 and 830 cm^{-1} for the liquid and solid samples, respectively (Fig. 4). An analogous shift in both the nondeuterated and N-deuterated molecules, *i.e.* an equivalent change in the corresponding force constants, reveals that hydrogen bond type and deuterium bond type interactions have the same magnitude.

Analysis of the INS spectrum of 1,3-dap (Fig. 3) allows us to observe signals not available to the optical techniques (Raman and FTIR). Firstly, the bands corresponding to the longitudinal and transversal acoustic modes (LAM and TAM, respectively), previously assigned by the authors,[24,25] are only detectable by

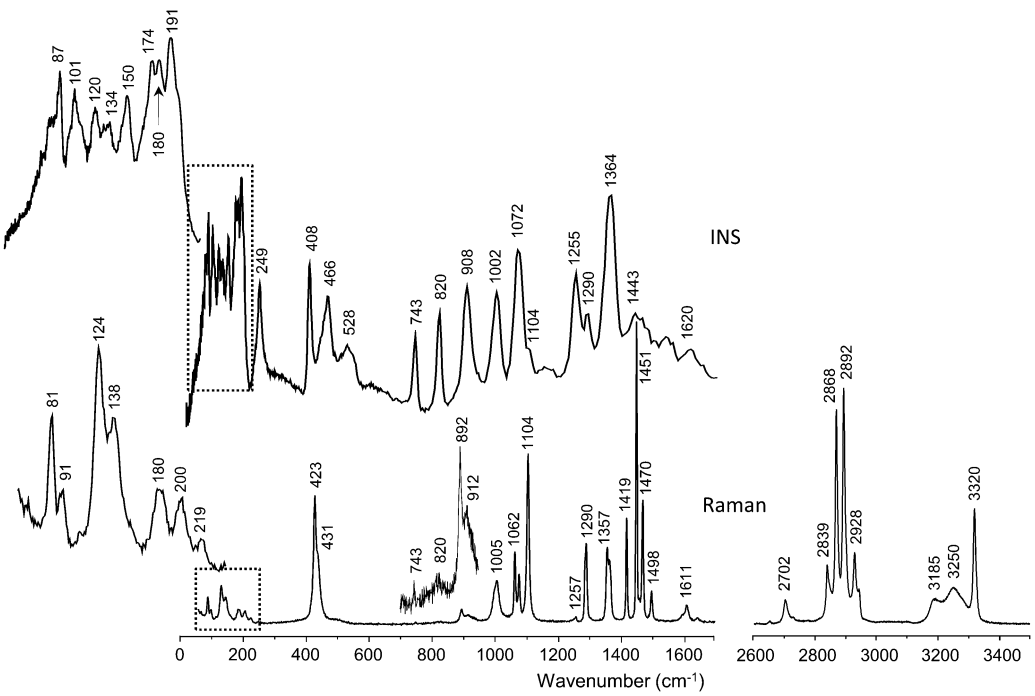

Fig. 3 INS (0–1700 cm^{-1}) and Raman (50–1700 cm^{-1} and 2600–3500 cm^{-1}) spectra of 1,3-diaminopropane in the solid phase.

Table 4 Vibrational (FTIR, Raman and INS) experimental and DFT-calculated harmonic wavenumbers (cm^{-1}) of 1,3-diaminopropane and its N-deuterated derivative in the liquid and solid states

Experimental									
1,3-DAP				1,3-DAP-ND_4					
Liquid		Solid		Liquid		Solid			
FTIR	Raman	Raman	INS	FTIR	Raman	Raman	Calculated[a]		Tentative assignment[b]
—		81	77	—		80	—		External mode
—		91	87	—		92	—		External mode
—		107	101	—			—		External mode
—		124	120	—		124	—		External mode
—		138	134	—		139	—		External mode
—			150	—			—		External mode
—		180	174	—		172	120	B_1	δCCN (out-of-plane; TAM2)
			180						
—		200	191	—		190	123	A_2	δCCN (out-of-plane; TAM1)
			~199						
—		219		—		209			
—			249	—			180	A_1	δNCCN (in-plane; LAM3)
—	276			—	271				
				—		324		A_2	τND_2
—	373			—	359				δNCC
—	412	423	408	—	398	411	395	A_1	δNCCN (in-plane; LAM1)
		431	~440				298	A_2	τNH_2
463			466				438	B_2	δNCCN (in-plane; LAM2)
515	513				490				δCCC + δ NCC
			528						τNH_2 (H-bonded)
						718			324 + 411
				723				B_2	ωND_2
						736			
769	~770	743	743			748	714	B_1	ρCH_2
				~765	768				ωND_2
					803	830		A_1	ωND_2
				~830	834				
	819	820	820				788	A_2	ρCH_2 + tCH_2 + tNH_2
875		892	908				888	B_2	ωNH_2
	912						875	A_1	ωNH_2
910					915				νCC
					947				ν CC
							954	B_1	tCH_2 + tNH_2
	976	1005	1002	979	984	996	995	B_2	ν_aCC (+ωNH_2)
				1019	1019				ν CC
				~1035	1039	1039			ν CC
1068	1070	1062	1072	1066	1070	1060	1044	A_1	ν_sCC
		1076				1072	1057	B_2	ν_aCN + ν_aCC
1095	1095	1104	1104	1097	1099	1084	1104	A_1	ν_sCN
					1153				tND_2
				1197	1196	1213			αND_2
				~1235	1243				tCH_2
		1257	1255	~1270	1276		1238	B_2	ωCH_2 + tCH_2
	1297	1290	1290	1300	1305	1309	1276	A_2	tCH_2
1317				1321					
1353	1357	1357					1338	A_1	tNH_2 + tCH_2
1389	1390	1364	1364	1369	1373	1368	1355	B_2	ωCH_2
		1419				1419			αCH_2
1435	1441	1451	1443	1442	1445	1450	1428	A_1	αCH_2
1471	1472	1470		1471	1479	1475	1455	A_1	αCH_2
		1498							
				1554					αNHD
1601							1598	B_2	αNH_2
	1603	1611	1620				1599	A_1	αNH_2
			—	2366	2370	2358			$\nu_s$$ND_2$ (D bonded)
			—	2424	2434	2431			$\nu_s$$ND_2$
			—	2506	2511	2483			$\nu_a$$ND_2$
~2690	~2690	2702			2722	2718			Overtone or combination mode
2760	2760		—		2755				Overtone or combination mode
		2839				~2845	2882	A_1	$\nu_s$$CH_2$
2855	2858	2868	—	2864	2871	2871	2904	A_1	$\nu_s$$CH_2$
		2892	—			2893	2917	B_1	$\nu_a$$CH_2$

Table 4 (*continued*)

Experimental									
1,3-DAP				1,3-DAP-ND_4					
Liquid		Solid		Liquid		Solid			
FTIR	Raman	Raman	INS	FTIR	Raman	Raman	Calculated[a]		Tentative assignment[b]
2926	2900	2928	—	2933	2911	2930	2953	B_1	ν_aCH_2
	~2930		—		2955				ν_aCH_2
~3190	3190	~3185	—						ν_sNH_2 (H bonded)
3285	3302	~3250	—				3263		ν_sNH_2
3359	3363	3320	—				3341		ν_aNH_2

[a] For the TTTT conformer (C_{2v} symmetry) of 1,3-diaminopropane at the mPW1PW/6-31G* level within the SCRF approach: calculated values scaled according to Merrick *et al.*:[45] 0.9499 and 0.9828, above and below 500 cm^{-1}, respectively. [b] Abbreviations: δ, deformation; τ, torsion; ω, wagging; t, twisting; ρ, rocking; α, scissoring; ν, stretching; s, symmetric; a, antissymmetric; TAM, transverse acoustic mode: LAM, longitudinal acoustic mode.

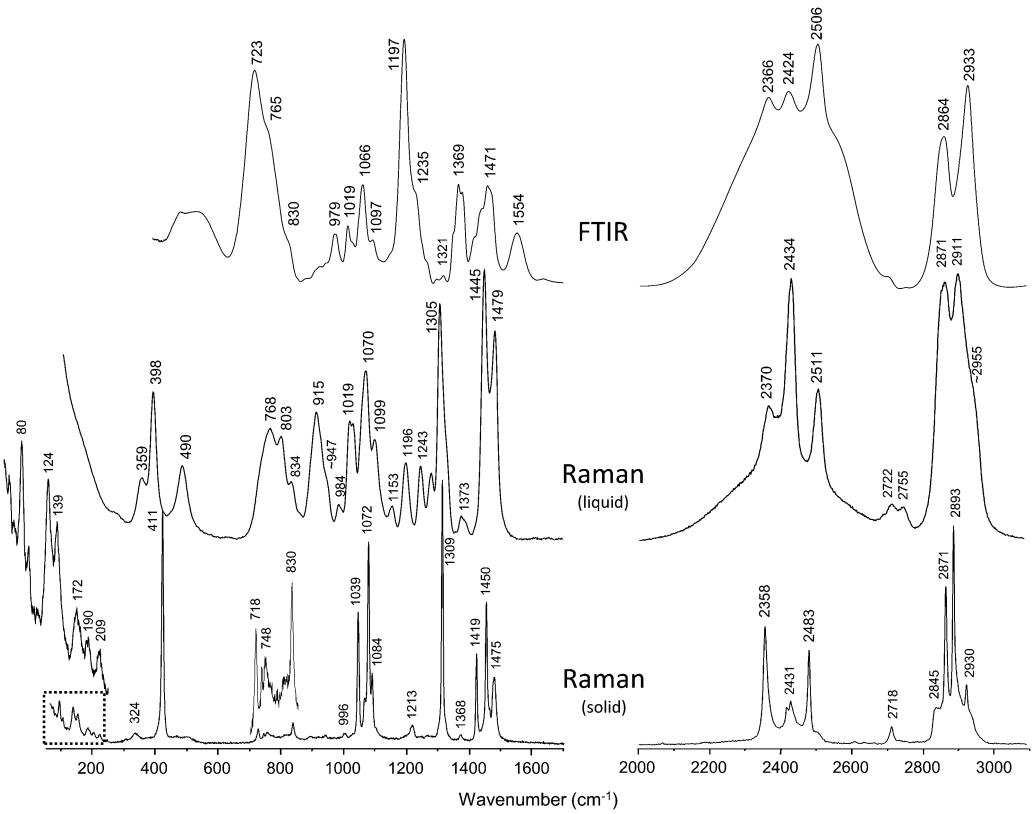

Fig. 4 FTIR (400–1700 and 2000–3100 cm^{-1}) and Raman (100–1700 and 2000–3100 cm^{-1}) spectra of 1,3-diaminopropane-N-d_4 in the liquid phase. Raman (50–1700 and 2000–3100 cm^{-1}) spectrum of 1,3-diaminopropane-N-d_4 in the solid phase.

INS (excluding LAM1 which is also observed in Raman). Also the INS signal at 743 cm^{-1}, ascribed to CH_2 rocking, is hardly seen in the Raman spectrum (Fig. 3). These observations are not surprising, since the vibrational techniques currently used are based on different physical processes: light scattering *vs.* neutron diffraction.

Regarding the Raman signals at 373/359 and 513/490 cm^{-1}, detected for the pure liquids (nondeuterated/N-deuterated, Fig. 2 and 4), they are completely absent from the solid phase spectra (Fig. 3 and 4). Actually, there is a fairly good correspondence between the δNCCCN values predicted for the all-*trans* geometry and the ones that remain on the solid phase vibrational spectra, which allow us to conclude that only the TTTT conformer is present in the solid sample, while the liquid consists of simultaneous equilibria of different conformers. In fact, when a *gauche* geometry around one of the CC bonds is considered, the skeletal deformation modes are predicted to be at 351 and 504 cm^{-1} (calculated values for the TGTT geometry), in close agreement with the band wavenumbers that disappear in the liquid → solid transition. It should be emphasized that the five most stable conformers (TTTT, TTTG, TGTT, TTGG′ and TGGG′) account for 53% of the liquid phase population (Table 2).

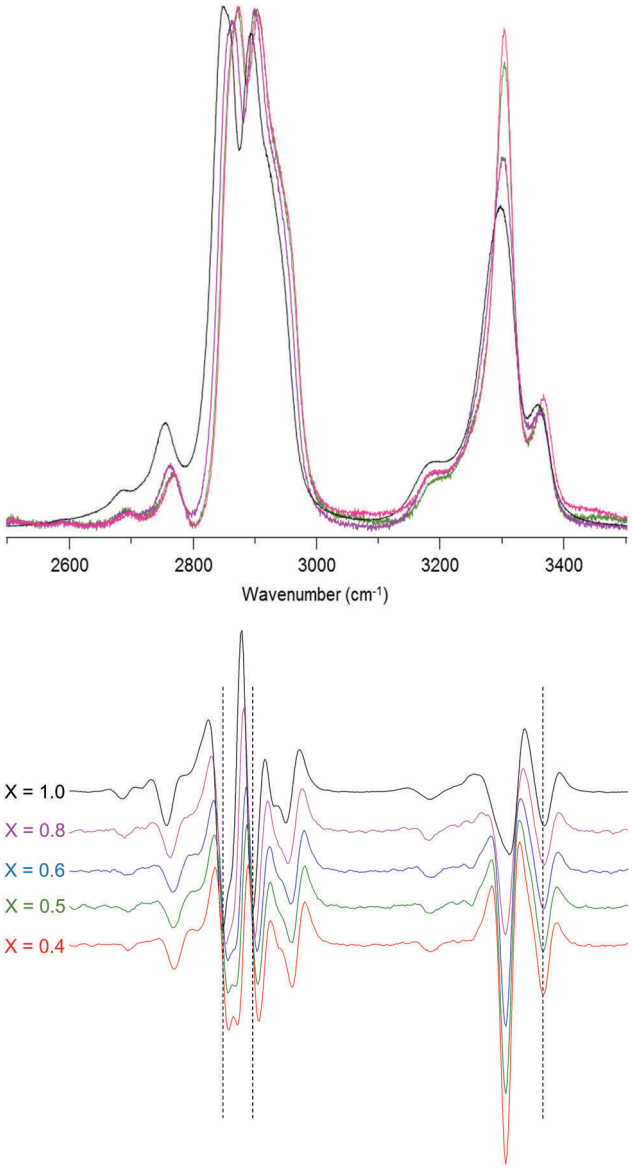

Fig. 5 Raman spectra (2500–3500 cm^{-1}) (upper) and the second derivative (bottom) of 1,3-diaminopropane aqueous solution at different molar fractions.

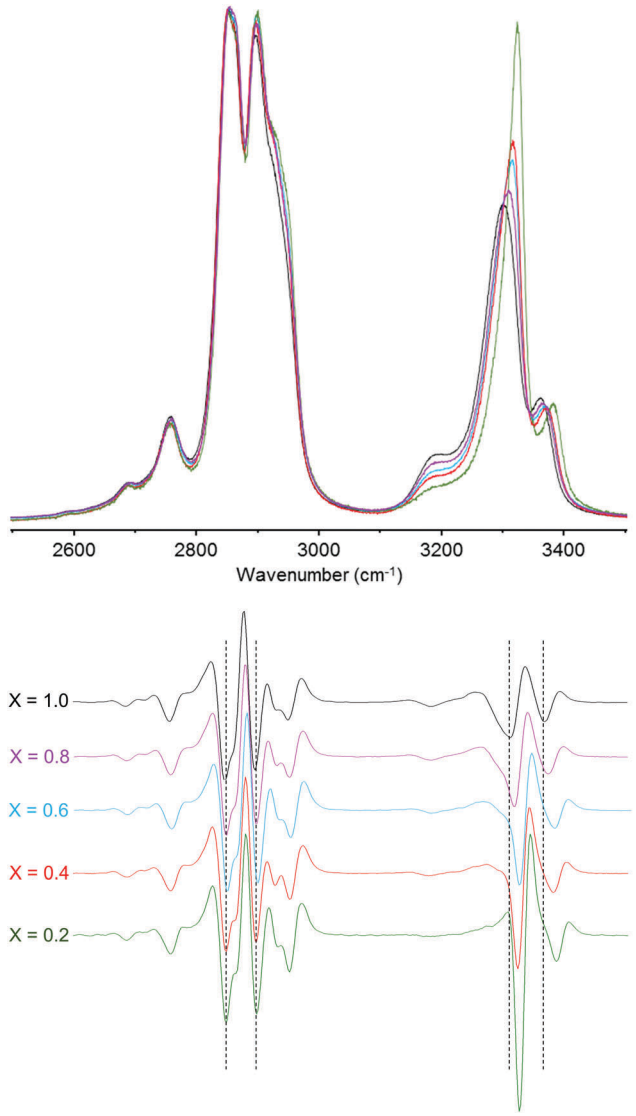

Fig. 6 Raman spectra (2500–3500 cm^{-1}) (upper) and the second derivative (bottom) of 1,3-diaminopropane/CCl_4 solution at different molar fractions.

Solvent effect

In order to assess the influence of environment polarity on the liquid 1,3-dap conformational equilibria, solutions of this diamine in both a polar solvent (water) and an apolar one (carbon tetrachloride) were prepared and the Raman spectra were recorded. Moreover, different molar fractions amine/solvent were used to evaluate possible concentration effects.

Regarding the aqueous solutions (Fig. S2, ESI†) some small changes could be observed upon dilution: (i) a 9 cm^{-1} upward shift of the δNCC mode at 373 cm^{-1}, assigned to an increased preference for a *gauche* arrangement around one of the CC skeletal bonds; (ii) the narrowing of the amine groups relating bands at 1603 and 3302 cm^{-1}, probably due to a lower conformational dispersion; and (iii) the apparent intensity decrease of the 910 cm^{-1} band, owing to the narrowing/downward shift of the NH_2 wagging mode that occurs in the same region and is clearly detected for both liquid (by FTIR, at 875 cm^{-1}) and solid sample (by Raman, at 892 cm^{-1}) spectra. A progressive shift to higher wavenumbers ($\leq$ 15 cm^{-1}) of the CH_2 symmetric and antisymmetric stretching bands with increasing molar fractions of water was also detected, due to the solvent polarity (Fig. 5). In fact, it is known that these stretching modes are sensitive to interchain interactions and to the polarity of the environment.[1,11,18] The observed Raman blue shift exposes a hydrophobic repulsive effect of water on the hydrophobic methylene groups of 1,3-dap,[17] which leads to an additional stabilisation of the conformers with a *gauche* arrangement of the alkyl chain.

Concerning the carbon tetrachloride solutions (Fig. S3, ESI†), the vibrational bands from the solvent hinder a clear observation of the solute signals and do not allow us to determine any

intensity changes in the 350–550 cm^{-1} range. However, the bands do not seem to be affected by dilution in this apolar solvent. Interestingly enough, the appearance of a new 1,3-dap band upon dilution at 877 cm^{-1} can be assigned to a change in conformational equilibrium, particularly to the presence of conformers not detected in the pure liquid. In the higher wavenumber region, in turn, there is an opposite behaviour to the one detected in aqueous solution: the methylene stretching signals do not undergo significant changes, while the amine stretching bands experience both a blue shift and an intensity enhancement with increasing dilution (Fig. 6). Moreover, a simultaneous intensity decrease of the 3200 cm^{-1} band, which is assigned to the $\nu_s NH_2$ mode when the amine group is involved in hydrogen bond type close contacts, is observed (Fig. 6). In fact, when the CCl_4 molar fraction is increased, 1,3-dap molecules "not connected", *i.e.* not involved in H-bonds (neither intra- nor intermolecular), are predominant.

$[H_3N\text{-}CH_2\text{-}CH_2\text{-}CH_2\text{-}NH_3]^{2+}$. Fig. 7 comprises Raman, FTIR and INS spectra of $[H_3N\text{-}CH_2\text{-}CH_2\text{-}CH_2\text{-}NH_3]^{2+}$ $2Cl^-$ while Fig. 8 presents the spectra of the N-deuterated molecule.

Experimental wavenumbers are presented in Table 5, along with the DFT calculated values for the TT conformer (C_{2v} symmetry), the hegemonic configuration (99%, Table 3).

For the solid samples, the occurrence of intermolecular interactions has a pronounced effect on the vibrational spectra. This is particularly important when amine systems are targeted, as they are prone to form extensive intermolecular hydrogen bond networks. By neglecting the effect of those interactions, significant deviations between the calculated and the experimental data are frequently observed.

Not surprisingly, the vibrational modes that are mostly affected concern the terminal $-NH_3^+$ groups as they are directly involved in intermolecular interactions. Among the 18 related modes, the most affected are, as previously found,[55,56] the stretching modes ($\nu_s NH_3$ and $\nu_{as} NH_3$) and the two torsional vibrations (τNH_3). These were found to be downward and upward shifted, respectively, by more than 300 cm^{-1}, due to N–H···Cl interactions. The effect on the deformation modes ($\delta_s NH_3$ and $\delta_{as} NH_3$) is comparatively insignificant, with an upward shift of less than 50 cm^{-1}. The NH_3^+ rocking modes (ρNH_3), on the other hand, are slightly more affected than δNH_3, with a negligible blue shift as compared to the νNH_3 and τNH_3 modes (between 56 and 86 cm^{-1}). Besides the $-NH_3^+$-related modes, only one other type of fundamental vibrations was found to be considerably affected by the presence of N–H···Cl interactions: the two NC stretching modes ($\nu_s NC$ and $\nu_{as} NC$) were

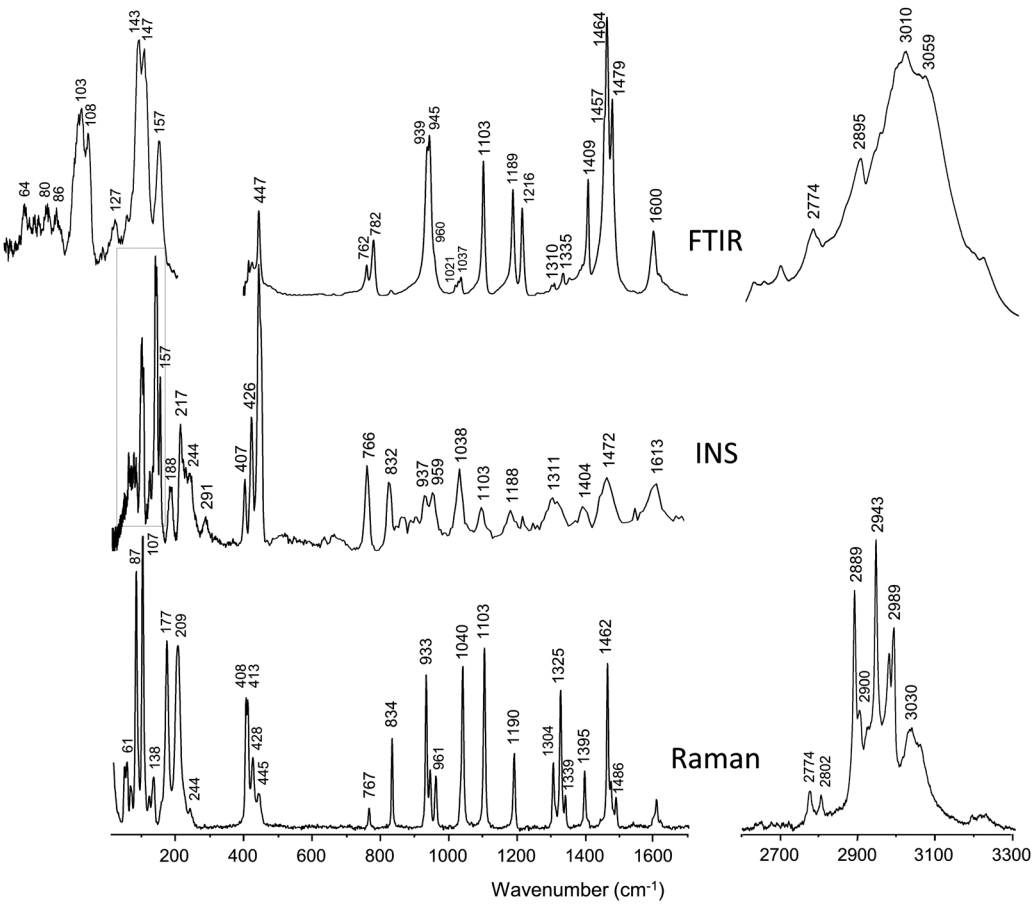

Fig. 7 FTIR (400–1700 and 2600–3300 cm^{-1}), INS (0–1700 cm^{-1}) and Raman (10–1700 and 2600–3300 cm^{-1}) spectra of solid 1,3-diaminopropane-N-h_6^{2+}·$2Cl^-$.

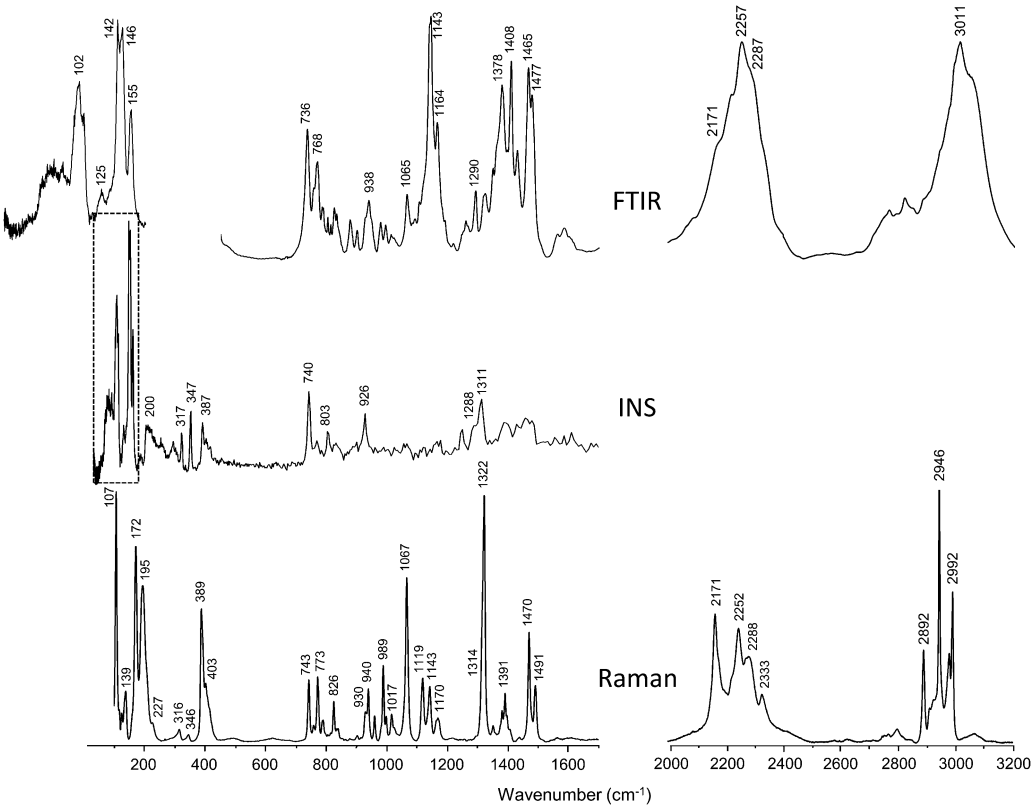

Fig. 8 FTIR (400–1700 and 2000–3200 cm^{-1}), INS (0–1700 cm^{-1}) and Raman (100–1700 and 2000–3200 cm^{-1}) spectra of solid 1,3-diaminopropane-N-d_6^{2+}·2Cl^-.

found to be upward shifted by more than 150 cm^{-1}, probably as a consequence of the proximity of the N–C bond to the N–H···Cl contacts.

As a consequence of the significant shifts promoted by N–H···Cl close contacts, several changes were observed in the relative ordering of the vibrational modes. If these are not considered, the assignment of the experimental vibrational spectra is inaccurate. A reported vibrational spectroscopic analysis of 1,2-ethylenediamine dihydrochloride ($[H_3N(CH_2)_2NH_3]^{2+}$ 2Cl^-)[55] allowed us to conclude that a precise theoretical forecast of the vibrational frequencies requires a molecular adduct comprising one cation surrounded by six chloride counterions, in a crystal structure based arrangement. However, such a molecular model tends to become too computationally expensive as the diamine size increases.

In order to overcome this limitation, a methodology has recently been developed and tested to correct the vibrational frequencies predicted for the isolated amine, in its cationic form, for the effects of the interactions with the counterions, without their explicit consideration in the calculation.[56] The correction factors to be used were determined by considering the whole series of α,ω-diamine hydrochlorides ($[H_3N(CH_2)_nNH_3]^{2+}$ 2Cl^-, n = 2–10 and 12; for more details see ref. 56).

Table 5 contains the experimental vibrational frequencies (FTIR, Raman and INS) and the corresponding assignments of solid $[H_3N(CH_2)_3NH_3]^{2+}$·2Cl^-. The theoretically predicted frequency values before and after correction for the effects of the intermolecular interaction, anharmonicity and incomplete electron correlation treatment are also listed for comparison. Note that the longitudinal and transversal skeletal modes (LAM and TAM) are not regarded in the methodology as they constitute a special group of vibrations.[56]

On the whole, it is found that correction for both intermolecular effects, by using the group correction factors previously defined,[56] and anharmonicity and incomplete electron correlation treatment, using the scaling factor of 0.9499 as suggested by Merrick *et al.*,[51] clearly improves the matching between observed and predicted vibrational frequencies. This is particularly obvious for the νNH_3 and τNH_3 modes, as they are more prone to be affected by N–H···Cl interactions, as mentioned above.

The νNH_3 modes, predicted around 3500 cm^{-1} for the isolated cation, are downward shifted to about 2900–2800 cm^{-1}. In other words, those modes are shifted to the spectral interval comprising the spectral features due to the CH_2 stretching modes (νCH_2). This is confirmed by the experimental data measured for the deuterated cationic molecule, namely by the disappearance of the bands observed between 2900 and 2774 cm^{-1} (Fig. 7 and 8; Table 5). Finally, calculations on the isolated $[H_3N(CH_2)_2NH_3]^{2+}$ cation predict the τNH_3 modes to occur at 235 and 238 cm^{-1}, far below the frequency of the spectral features observed to disappear upon deuteration – 413 and 447 cm^{-1} (Fig. 7 and 8). The disappearance of these two spectral features is accompanied by the detection of new bands around 317 and 347 cm^{-1} (Fig. 8). Yet, correction of the 235 and 238 cm^{-1} calculated values yields

Table 5 Vibrational (FTIR, Raman and INS) experimental and DFT-calculated harmonic wavenumbers (cm^{-1}) of $H_3N(CH_2)_3NH_3^{2+}\cdot 2Cl^-$ and its N-deuterated derivative in the solid state

$H_3N(CH_2)_3NH_3^{2+}$					$D_3N(CH_2)_3ND_3^{2+}$						
Exp.			Calc.[a]		Exp.			Calc.[a]			
FTIR	Raman	INS	(1)	(2)	FTIR	Raman	INS	(1)	(2)	Sym	Tentative assignment[b]
—	53		—	—	—			—	—		External mode
—	61	64	—	—	—			—	—		External mode
—	71		—	—	—			—	—		External mode
—		80	—	—	—			—	—		External mode
—	87	86	—	—	—		85	—	—		External mode
—	107	103	—	—	—	107	102	—	—		External mode
		108					107				
—	126	127	—	—	—	126	125	—	—		External mode
—	138	135	—	—	—	139		—	—		External mode
—		143	—	—	—		142	—	—		External mode
		147					146				
—		157	105	[c]	—		155	92	[c]	A_2	δNCCN (TAM2)
—	177	188	122	[c]	—	172	181	113	[c]	B_1	δNCCN (TAM1)
—	209	217	188	[c]	—	195	200	171	[c]	A_1	δNCCN (LAM3)
—	244	244	—	—	—	227		—	—		(108 + 147 cm^{-1})
—		291	—	—	—		290	—	—		(143 + 157 cm^{-1})
—	408	407	386	[c]	—	389	387	363	[c]	A_2	δNCCN (LAM1)
	413										
427	428	426	417	[c]	—	403	399	381	[c]	B_2	δNCCN (LAM2)
447	445	447	235	549	—	316	317	182	425	B_1	τNH_3 (τND_3)
			238	556	—	346	347	186	435	A_2	τNH_3 (τND_3)
762	767	766	772	777	736	743	740	731	736	B_1	ρNH_3 (ρND_3) + ρCH_2
782											
	834	832	836	842				723	728	A_2	ρNH_3 (ρND_3) + ρCH_2
939	933	937	926	932	768	773	766	760	765	A_1	ρNH_3 (ρND_3)
945	944										
960	961	959	951	958	786	789	803	802	808	B_1	ρNH_3 (ρND_3) + $t CH_2$ + ρCH_2
1030	1040	1038	1030	1037	825	826835	828	818	824	B_2	ρNH_3 (ρND_3)
1037					832						
					927	930	926	943	950	A_2	ρND_3 + ρCH_2 + $t CH_2$
					938	940					
						960					
					978	989		1075	991	B_2	$\nu_a CC$
					994	998					
1021			921	1024	1012	1017		912	1014	B_2	$\nu_a NC$
1103	1103	1103	1116	1124	1065	1067				B_2	ρNH_3 + $\nu_a CC$
		1016	1129					970	1078	A_1	$\nu_s NC$
1189	1190	1188	1243	1181		1119		1197	1137	B_1	ρCH_2 + ρNH_3 (ρND_3)
1216		1224	1204	1212	1143	1143		1132	1140	A_1	ρNH_3 (ρND_3) + $\nu_s CC$
	1304	1311	1355	1287			1247	1317	1251	A_2	$t CH_2$
1310			1373	1304	1291		1288	1358	1290	B_2	ωCH_2
	1325	1326	1390	1320		1322		1386	1317	A_2	$t CH_2$
1335	1339		1405	1335	1321	1314	1311	1384	1315	B_1	$t CH_2$
	1395		1462	1389	1378	1381	1392	1454	1381	A_1	ωCH_2
1409		1404	1476	1402	1408	1391		1476	1402	B_2	ωCH_2
1457	1462	1472	1523	1447	1465	1470	1460	1523	1447	A_1	αCH_2
1464	1472										
1479	1486		1537	1460	1477	1491	1479	1537	1460	A_1	αCH_2
			1589	1524				1220	1170	B_2	$\delta_s NH_3$ ($\delta_s ND_3$)
			1591	1526				1223	1173	A_1	$\delta_s NH_3$ ($\delta_s ND_3$)
1600	1604	1613	1704	1635	1164	1170	1164	1228	1178	B_2	$\delta_{as} NH_3$ ($\delta_{as} ND_3$)
			1706	1637				1229	1179	A_1	$\delta_{as} NH_3$ ($\delta_{as} ND_3$)
			1711	1642				1230	1180	A_2	$\delta_{as} NH_3$ ($\delta_{as} ND_3$)
			1711	1642				1231	1181	B_1	$\delta_{as} NH_3$ ($\delta_{as} ND_3$)
2895			3406	2847	2171			2443	2042	B_2	$\nu_s NH_3$ ($\nu_s ND_3$)
	2900		3408	2849		2171		2445	2044	A_1	$\nu_s NH_3$ ($\nu_s ND_3$)
	3030		3490	2917	2257	2252		2574	2152	B_2	$\nu_{as} NH_3$ ($\nu_{as} ND_3$)
			3491	2918				2575	2152	A_1	$\nu_{as} NH_3$ ($\nu_{as} ND_3$)
	3053		3502	2927		2288		2585	2161	A_2	$\nu_{as} NH_3$ ($\nu_{as} ND_3$)
3059			3503	2928	2287			2585	2161	B_1	$\nu_{as} NH_3$ ($\nu_{as} ND_3$)
	2889		3077	2923	2896	2892		3077	2923	A_1	$\nu_s C^7H_2$
	2943		3129	2972		2946		3129	2972	B_1	$\nu_{as} C^7H_2$
	2976		3134	2977		2980		3134	2977	B_2	$\nu_s CH_2$
	2989		3137	2980		2992		3137	2980	A_1	$\nu_s CH_2$

Table 5 (*continued*)

$H_3N(CH_2)_3NH_3^{2+}$					$D_3N(CH_2)_3ND_3^{2+}$						
Exp.			Calc.[a]		Exp.			Calc.[a]			
FTIR	Raman	INS	(1)	(2)	FTIR	Raman	INS	(1)	(2)	Sym	Tentative assignment[b]
3010			3201	3041	3011			3201	3041	B_1	$\nu_{as}CH_2$
		3197	3037					3197	3037	A_2	$\nu_{as}CH_2$

[a] Column (1) – uncorrected and unscaled mPW1PW/6-31G* calculated frequencies of isolated $H_3N(CH_2)_3NH_3^{2+}$ (TT conformer; C_{2v} symmetry); column (2) – corrected (using the group correction factors reported in ref. 52) and scaled (using a scaling factor of 0.9499 as suggested by Merrick *et al.*[50]) mPW1PW/6-31G* calculated frequencies for isolated $H_3N(CH_2)_3NH_3^{2+}$ (TT conformer; C_{2v} symmetry). [b] δ, deformation; τ, torsion; ω, wagging; t, twisting; ρ, rocking; α, scissoring; ν, stretching; s, symmetric; a, antissymmetric; TAM, transverse acoustic mode: LAM, longitudinal acoustic mode. [c] Not calculated using this method, see the text.

the wavenumbers 549 and 556 cm^{-1}, much closer to the experimental values pointed out by the deuteration studies (413 and 447 cm^{-1}).

Conclusion

In the present work, a conformational analysis of one of the smallest alkyl polyamines, 1,3-diaminopropane, was performed by complementary vibrational techniques, both optical – FTIR and Raman – and inelastic neutron scattering, coupled to DFT calculations.

These calculations, using the mPW1PW functional and the 6-31G(d) basis set, were carried out for four distinct systems: isolated molecule and condensed phase, and solutions in water and carbon tetrachloride (at the SCRF-PCM level). For each environment, more than two dozen real minima in the potential energy surface were found. The most stable conformers, both in the gaseous phase and in CCl_4 solution, were GGG′G and TG′GG′. For both the liquid phase and the aqueous solution, in turn, TTTT, TGTT and TTTG were the predominant species.

Vibrational spectra were recorded for the pure compound (liquid and solid phases), carbon tetrachloride and aqueous solutions (at different molar fractions), as well as for the N-ionised and N-deuterated species. Assignment of the vibrational patterns was carried out in the light of the corresponding calculated harmonic vibrational frequencies, isotopic substitution (N-deuteration) and by comparison with similar molecules previously studied by the authors (*e.g.* 1,2-diaminoethane[9]).

The experimental spectra corroborate the assessment based on the theoretical calculations: (i) liquid 1,3-diaminopropane (either pure or in solution) consists of a simultaneous equilibria of different conformers, some of them with skeletal *gauche* arrangements; (ii) in the solid samples (both 1,3-diaminopropane and its N-protonated counterpart) only the all-*trans* conformers are present; and (iii) although the conformational equilibria in aqueous solution is similar to that of pure liquid, a hydrophobic repulsive interaction between the water molecules and the methylene groups of 1,3-dap takes place leading to an additional stabilisation of the conformers with a *gauche* arrangement of the alkyl chain and a slightly lower conformational dispersion.

This type of conformational study on compounds with putative pharmacological interest is of utmost relevance for understanding their structure–activity relationships aiming at future applications in the field of biomedicine. In the particular case of 1,3-diaminepropane, the results presently obtained allow it to be considered as a very suitable ligand for Pt(II) and Pd(II) coordination, yielding complexes (either mono- or dinuclear) with a potential antitumor ability (through DNA-binding), attending to the conformational characteristics currently unveiled. This will greatly contribute to the rational design of improved metal-based anticancer agents with higher efficacy coupled to lower toxicity and acquired resistance.

Acknowledgements

The authors thank financial support from the Portuguese Foundation for Science and Technology – UID/Multi/00070/2013 and PTDC/QEQ-MED/1890/2014 (within Project 3599 – Promote Scientific Production and Technological Development as well as the Formation of Thematic Networks (3599-PPCDT) – jointly financed by the European Community Fund FEDER). The STFC Rutherford Appleton Laboratory is thanked for access to neutron beam facilities. Acknowledgements are also due to CICECO, University of Aveiro, Portugal, for access to computational facilities (Gaussian 09 program).

Notes and references

1 J. J. C. Teixeira-Dias, L. A. E. Batista de Carvalho, A. M. Amorim da Costa, I. M. S. Lampreia and E. F. G. Barbosa, *Spectrochim. Acta, Part A*, 1986, **42**, 589.
2 N. Sato, Y. Hamada and M. Tsuboi, *Spectrochim. Acta, Part A*, 1987, **43**, 943.
3 L. A. E. Batista de Carvalho, A. M. Amorim da Costa, M. L. Duarte and J. J. C. Teixeira-Dias, *Spectrochim. Acta, Part A*, 1988, **44**, 723.
4 J. R. Durig, W. B. Beshir, S. E. Godbey and T. J. Hizer, *J. Raman Spectrosc.*, 1989, **20**, 311.
5 L. A. E. Batista de Carvalho, A. M. Amorim da Costa and J. J. C. Teixeira-Dias, *THEOCHEM*, 1990, **64**, 327.
6 L. A. E. Batista de Carvalho, J. J. C. Teixeira-Dias and R. Fausto, *Struct. Chem.*, 1990, **1**, 533.

7 L. R. Schmitz and N. L. Allinger, *J. Am. Chem. Soc.*, 1990, **112**, 8307.
8 L. A. E. Batista de Carvalho and J. J. C. Teixeira-Dias, *J. Raman Spectrosc.*, 1995, **26**, 653.
9 L. A. E. Batista de Carvalho, L. E. Lourenço and M. P. M. Marques, *J. Mol. Struct.*, 1999, **482**, 639.
10 M. P. M. Marques and L. A. E. Batista de Carvalho, in *COST 917: Biogenically Active Amines in Food*, ed. D. M. L. Morgan, A. White, F. Sanchez-Jimenez and S. Bardocz, Book Series: European Commission – Science Research Development, 2000, vol. 4, pp. 122–129.
11 A. M. Amorim da Costa, M. P. M. Marques and L. A. E. Batista de Carvalho, *J. Raman Spectrosc.*, 2003, **34**, 357.
12 J. R. Durig, C. Zheng, T. K. Gounev, W. A. Herrebout and B. J. van der Veken, *J. Phys. Chem. A*, 2006, **110**, 5674.
13 O. Alver and C. Parlak, *J. Theor. Comput. Chem.*, 2010, **9**, 667.
14 S. Padrão, S. M. Fiuza, A. M. Amado, A. M. Amorim da Costa and L. A. E. Batista de Carvalho, *J. Phys. Org. Chem.*, 2011, **24**, 110.
15 M. Tursun, G. Kesan, C. Parlak and M. Senyel, *Spectrochim. Acta, Part A*, 2013, **114**, 668.
16 T. M. Silva, S. M. Fiuza, M. P. M. Marques, L. A. E. Batista de Carvalho and A. M. Amado, *Spectrochim. Acta, Part A*, 2016, **157**, 227.
17 M. Caceres, A. Lobato, N. J. Mendoza, L. J. Bonales and V. G. Baonza, *Phys. Chem. Chem. Phys.*, 2016, **18**, 26192.
18 A. M. Amorim da Costa, M. P. M. Marques and L. A. E. Batista de Carvalho, *Vib. Spectrosc.*, 2004, **35**, 165.
19 H. M. Wallace, A. V. Fraser and A. Hughes, *Biochem. J.*, 2003, **376**, 1.
20 J. E. Seely and A. E. Pegg, *Biochem. J.*, 1983, **216**, 701.
21 E. I. Salim, H. Wanibuchi, K. Morimura, S. Kim, Y. Yano, S. Yamamoto and S. Fukushina, *Carcinogenesis*, 2000, **21**, 195.
22 E. W. Gerner and F. L. Meyskens, *Nat. Rev. Cancer*, 2004, **4**, 781.
23 S. L. Nowotarski, P. M. Woster and R. A. Casero, Jr., *Expert Rev. Mol. Med.*, 2013, **15**, e3.
24 M. P. M. Marques, L. A. E. Batista de Carvalho and J. Tomkinson, *J. Phys. Chem. A*, 2002, **106**, 2473.
25 L. A. E. Batista de Carvalho, M. P. M. Marques and J. Tomkinson, *J. Phys. Chem. A*, 2006, **110**, 12947.
26 V. L. Gein, V. V. Yushkov, N. N. Kasimova, M. A. Panina, N. S. Rakshina, L. V. Strelkova and E. V. Voronina, *Pharm. Chem. J.*, 2007, **41**, 367.
27 C. G. Van Kralingen, J. Reedijk and A. L. Spek, *Inorg. Chem.*, 1980, **19**, 1481.
28 A. Alvarez-Valdés, J. M. Pérez, I. López-Solera, R. Lannegrand, J. M. Continente, P. Amo-Ochoa, M. J. Camazón, X. Solans, M. Font-Bardía and C. Navarro-Ranninger, *J. Med. Chem.*, 2002, **45**, 1835.
29 H. Silva, C. V. Barra, C. França da Costa, M. Vieira de Almeida, E. T. César, J. N. Silveira, A. Garnier-Suillerot, F. C. Silva de Paula, E. C. Pereira-Maia and A. P. S. Fontes, *J. Inorg. Biochem.*, 2008, **102**, 767.
30 A. L. M. Batista de Carvalho, S. M. Fiuza, J. Tomkinson, L. A. E. Batista de Carvalho and M. P. M. Marques, *Spectrosc. – Int. J.*, 2012, **27**, 403.
31 J. Ferlay, I. Soerjomataram, R. Dikshit, S. Eser, C. Mathers, M. Rebelo, D. M. Parkin, D. Forman and F. Bray, *Int. J. Cancer*, 2015, **136**, E359.
32 L. Kelland, *Nat. Rev. Cancer*, 2007, **7**, 573.
33 N. P. Farrell, *Curr. Top. Med. Chem.*, 2011, **11**, 2623.
34 Y. Li, Y. Li, J. Li, G. Pi and W. Tan, *OncoTargets Ther.*, 2014, **7**, 1361.
35 M. T. Truong, J. Winzelberg and K. W. Chang, *Int. J. Pediatr. Otorhi.*, 2007, **71**, 1631.
36 X. Yao, K. Panichpisal, N. Kurtzman and K. Nugent, *Am. J. Med. Sci.*, 2007, **334**, 115.
37 S. M. Fiuza, A. M. Amado, P. J. Oliveira, V. A. Sardão, L. A. E. Batista de Carvalho and M. P. M. Marques, *Lett. Drug Des. Discovery*, 2006, **3**, 149.
38 A. S. Soares, S. M. Fiuza, M. J. Gonçalves, L. A. E. Batista de Carvalho, M. P. M. Marques and A. M. Urbano, *Lett. Drug Des. Discovery*, 2007, **4**, 460.
39 C. Mitchell, P. Kabolizadeh, J. Ryan, J. D. Roberts, A. Yacoub, D. T. Curiel, P. B. Fisher, M. P. Hagan, N. P. Farrell, S. Grant and P. Dent, *Mol. Pharmacol.*, 2007, **72**, 704.
40 A. Hegmans, J. Kasparkova, O. Vrana, L. R. Kelland, V. Brabec and N. P. Farrell, *J. Med. Chem.*, 2008, **51**, 2254.
41 R. Tummala, P. Diegelman, S. M. Fiuza, L. A. E. Batista de Carvalho, M. P. M. Marques, D. L. Kramer, K. Clark, S. Vulcic, C. W. Porter and L. Pendyala, *Oncol. Rep.*, 2010, **24**, 15.
42 S. M. Fiuza, J. Holy, L. A. E. Batista de Carvalho and M. P. M. Marques, *Chem. Biol. Drug Des.*, 2011, **77**, 477.
43 S. M. Fiuza, A. M. Amado, S. F. Parker, M. P. M. Marques and L. A. E. Batista de Carvalho, *New J. Chem.*, 2015, **39**, 6274.
44 A. L. M. Batista de Carvalho, M. Pilling, P. Gardner, J. Doherty, G. Cinque, K. Wehbe, C. Kelley, L. A. E. Batista de Carvalho and M. P. M. Marques, *Faraday Discuss.*, 2016, **187**, 273.
45 S. F. Parker, F. Fernandez-Alonso, A. J. Ramirez-Cuesta, J. Tomkinson, S. Rudic, R. S. Pinna, G. Gorini and J. Fernández Castañon, *J. Phys.: Conf. Ser.*, 2014, **554**, 012003.
46 ISIS – STFC – TOSCA, http://www.isis.stfc.ac.uk/instruments/tosca/, 2017 accessed 01.03.17.
47 M. J. Frisch, G. W. Trucks, H. B. Schlegel, G. E. Scuseria, M. A. Robb, J. R. Cheeseman, G. Scalmani, V. Barone, G. A. Petersson, H. Nakatsuji, M. Caricato, X. Li, A. Marenich, J. Bloino, B. G. Janesko, R. Gomperts, B. Mennucci, H. P. Hratchian, J. V. Ortiz, A. F. Izmaylov, J. L. Sonnenberg, D. Williams-Young, F. Ding, F. Lipparini, F. Egidi, J. Goings, B. Peng, A. Petrone, T. Henderson, D. Ranasinghe, V. G. Zakrzewski, J. Gao, N. Rega, G. Zheng, W. Liang, M. Hada, M. Ehara, K. Toyota, R. Fukuda, J. Hasegawa, M. Ishida, T. Nakajima, Y. Honda, O. Kitao, H. Nakai, T. Vreven, K. Throssell, J. A. Montgomery, Jr., J. E. Peralta, F. Ogliaro, M. Bearpark, J. J. Heyd, E. Brothers, K. N. Kudin, V. N. Staroverov, T. Keith, R. Kobayashi, J. Normand, K. Raghavachari, A. Rendell, J. C. Burant, S. S. Iyengar, J. Tomasi, M. Cossi, J. M. Millam, M. Klene, C. Adamo,

R. Cammi, J. W. Ochterski, R. L. Martin, K. Morokuma, O. Farkas, J. B. Foresman and D. J. Fox, *Gaussian 09, Revision A.02*, Gaussian, Inc., Wallingford CT, 2016.
48 C. Adamo and V. Barone, *J. Chem. Phys.*, 1998, **108**, 699.
49 J. P. Perdew, K. Burke and Y. Wang, *Phys. Rev. B: Condens. Matter Mater. Phys.*, 1996, **54**, 16533.
50 P. C. Hariharan and J. A. Pople, *Theor. Chim. Acta*, 1973, **28**, 213.
51 J. P. Merrick, D. Moran and L. Radom, *J. Phys. Chem. A*, 2007, **111**, 11683.
52 J.-D. Chai and M. Head-Gordon, *Phys. Chem. Chem. Phys.*, 2008, **10**, 6615.
53 Y. Zhao and D. G. Truhlar, *Theor. Chem. Acc.*, 2008, **120**, 215.
54 G. D. Purvis III and R. J. Bartlett, *J. Chem. Phys.*, 1982, **76**, 1910.
55 A. M. Amado, J. C. Otero, M. P. M. Marques and L. A. E. Batista de Carvalho, *ChemPhysChem*, 2004, **5**, 1837.
56 S. M. Fiuza, T. M. Silva, M. P. M. Marques, L. A. E. Batista de Carvalho and A. M. Amado, *J. Mol. Model.*, 2015, **21**, 266.